Clues on the obscured active nucleus of NGC 1365[*]

Hartmut Schulz[1], Stefanie Komossa[2], Clemens Schmitz[1,3], and Anita Mücke[4]

[1] Astronomisches Institut, Ruhr-Universität, D-44780 Bochum, Germany
[2] Max-Planck-Institut für Extraterrestrische Physik, Postfach 1603, D-85740 Garching, Germany
[3] Institut für Geowissenschaften, Universität Jena, Burgweg 11, D-07749 Jena, Germany
[4] Department of Physics and Mathematical Physics, University of Adelaide, Adelaide, SA 5005, Australia

Abstract. We have analyzed optical spectra (ESO-CASPEC) from the composite starburst-Seyfert galaxy NGC 1365 taken on the nucleus and the following positions (relative to nucleus): $2''$N, $2''$W; $2''$S; $4''$S; $5''$S; $10''$S and $20''$W. A nuclear broad-line component indicative of the AGN source is confirmed in Hβ and Hα. Narrow-line widths vary between 150 and 200 km s^{-1}. Extranuclear line ratios in the observed regions are mostly consistent with the lines being formed in HII regions. One of the exceptions is a rise of [OIII]λ5007/Hβ from 0.5 to 5 within $5''$ (from west to east) across the nucleus suggesting the transition from gas ionized by stars to gas ionized by the active nucleus.

Faint emission-line gas observed $20''$ W of the nucleus (called region II) shows line ratios lying in the AGN part of diagnostic diagrams. While at first glance shocks by bar streaming motions appear to be a suggestive explanation for these line ratios we stress that there is no positive evidence for the velocities > 300 km s^{-1} required for this mechanism. Another, presently more likely, explanation is that region II belongs to the far cone of the bipolar nuclear outflow which can be glimpsed through the dusty disk. Photoionization of a single-density cloud system by a diluted AGN continuum reproduces the measured line ratios, but leads via the ionization parameter to an intrinsic Hα luminosity of the obscured AGN of $\sim 10^{42}$ erg s^{-1} of which less than $\sim 4\%$ are observed in the central few arcseconds. Dust obscuration could explain Hα but its concomitant gas column cannot account for the lack of Seyfert-1 typical hard X-rays from the nucleus.

Key words: galaxies: active – galaxies: general – galaxies: individual: NGC 1365 – galaxies: nuclei – galaxies: Seyfert – galaxies: starburst

1. Introduction

NGC 1365 is a bright barred spiral in the southern hemisphere. It has been a target of numerous optical studies (e.g., Burbidge & Burbidge 1960; Burbidge et al. 1962; Osmer et al. 1974; Alloin & Kunth 1979; Pagel et al. 1979; Phillips & Frogel 1980; Veron et al. 1980; Blackman 1981; Edmunds & Pagel 1982; Phillips et al. 1983; Jörsäter et al. 1984a, b; Diaz et al. 1985; Teuben et al. 1986; Edmunds et al. 1988; Roy & Walsh 1988, Saikia et al. 1994). Lindblad et al. (1996a, b) provided comprehensive maps and models of the galactic velocity field. Utilizing HST-FOC images, Kristen et al. (1997) described the morphology of the brightest circumnuclear spots on the $0''.1$ scale.

Broad emission-line Hα indicative of a Seyfert-1.5 galaxy was detected by Veron et al. (1980). HII region-like *extranuclear* line ratios are common indicating widespread circumnuclear starformation. A circumnuclear ring of optical and radio hot spots, in many spectral bands challenging the nucleus in flux level, as well as abundant molecular gas corroborate the starburst character (Sandqvist et al. 1995, Saikia et al. 1994).

Narrow-line AGN characteristics are found via extranuclear [OIII]λ5007 enhancements, which roughly trace a wide conical region (Phillips et al. 1983; Jörsäter & Lindblad 1989; Storchi-Bergmann & Bonatto 1991; Kristen et al. 1997). Aside from the broad Balmer-line component, the nuclear spot does not exhibit an AGN-typical high-ionization narrow-line spectrum and its large Hα/Hβ ratio indicates significant extinction ($A_V = 3^{\rm m} - 4^{\rm m}$; Alloin et al. 1981). Broad-band polarization data are more typical for a Seyfert-2 than for a Seyfert-1, and the E-vector coincides with the outflow-cone axis rather than with any disk property of the galaxy (Brindle et al. 1990).

In addition, the presence of an AGN is indicated by a hard powerlaw-like component in *ASCA* and *ROSAT* X-ray spectra and conspicuous FeK line emission unlike that found in starburst galaxies (Iyomoto et al. 1997, Komossa & Schulz 1998a, b). As pointed out by Komossa & Schulz (1998a, b), the ratios of Hα to the mid-infrared continuum and to the hard-X radiation differ considerably from those seen in a large sample of representative broad-line AGNs (Ward et al. 1988) which may only be reconciled by a complicated scenario of selectively different amounts of obscuration and starburst admixtures. Any simple version of the 'unified model' appears to fail for NGC 1365.

In the present note, we communicate a few spectroscopic results that lead a step further to understand the central structure

---

of this galaxy. In particular, we address the important question how luminous the obscured AGN might be.

Basic data of NGC 1365 are adopted from the compilation in Table 2 of Schulz et al. 1994 (hereafter: Paper I): $v_{sys} = (1639 \pm 20)\,\mathrm{km\,s^{-1}}$ implying a distance of 19.8 Mpc (linear scale 96 pc/″) with $H_0 = 75\,\mathrm{km\,s^{-1}\,Mpc^{-1}}$ and the virgocentric model of Kraan-Korteweg (1986). Recent HST borne cepheid data lead to an insignificantly smaller distance of 18.6 ± 1.9 Mpc (Madore et al. 1998; an additional 1.9 Mpc systematic error may be present).

2. Acquisition of the optical spectra and reductions

The spectra described here were taken by A.M. during the period August 25–28 in 1993 using the CASPEC echelle spectrograph attached to the short camera at the Cassegrain focus of the ESO 3.6m telescope on La Silla. The data reductions were carried out by C.S. A log of the observations is given in Table 1. The detector was a Tektronix CCD chip with 27 μm wide pixels (CCD #32). The spatial resolution element is 0.″648 px^{-1} (corresponding to the pixel size perpendicular to the direction of dispersion or width of one row in the final frame; Pasquini 1993). Seeing and telescope properties limited the spatial resolution to 2″ which was determined by the width of standard star spectra on the focal exposures. The pointing positions were chosen by moving the telescope relative to the visually centered nucleus.

The spectral resolution as determined by the FWHM of night sky lines is 0.4 Å (corresponding to $\sim 20\,\mathrm{km\,s^{-1}}$) on the average. The CCD frames were bias subtracted. A full flat-field division could not be carried out because of a shift of the flat field exposure relative to the object frames. Fortunately, the effect of flat-field reduction in the overlapping regions turned out to be minor so that we could ignore this step. Other steps like determining the positions of the spectral orders as well as scattered-light subtraction were carried out as described in the ESO-MIDAS echelle software bundle which we employed. Extinction correction with Tüg's (1977) curve and a relative flux calibration employing the standard star Kopf 27 (Stone & Baldwin 1971) were applied to determine *relative* line intensities. The low resolution of the published standard star flux values caused some problems in pasting the orders continuously together. These difficulties were solved by manual interaction within the fitting process. By integrations over the finally reduced standard star spectra it was verified that the published flux values could be reproduced to < 3%. However, due to partial cirrus and a narrow slit we refrain from giving absolute flux values for the galaxy spectra.

The usual thorium-argon spectra (D'Odorico et al. 1987) fitted by third-order polynomials were used for wavelength calibration. The major deviation from the general MIDAS echelle reduction scheme was to extract individual rows from the orders and paste them together along wavelength. Usually, the software assumes that a single average spectrum is extracted. The strong sensitivity decreases of the individual orders towards the rims perpendicular to the dispersion had to be corrected for in order to be able to compare the different row spectra. To this end, ten

Table 1. Journal of the spectroscopic observations. Slit $\widehat{=}$ Pos. of slit center relative to nucleus. Range: red $\widehat{=}$ 5700–8400 Å, blue $\widehat{=}$ 4200–5700 Å. $t(\exp)$ = exposure time in s.

No.	Date	Slit	Range	$t(\exp)$
S1	26-Aug-93	2″N, 2″W	red	2722
S2	27-Aug-93	20″W	red	3600
S3	27-Aug-93	20″W, 2″S	red	3600
S4	27-Aug-93	2″S	red	2680
S5	27-Aug-93	4″S	red	2400
S6	28-Aug-93	5″S	blue	3600
S7	28-Aug-93	10″S	blue	3600
S8	28-Aug-93	nucl.	blue	3600
S9	28-Aug-93	20″W	blue	3600

night-sky lines were used to determine an average 'vignetting' profile under the assumption that the night-sky line brightness should not vary perpendicular to the dispersion. This procedure works well, but the rows close to the rims are too noisy so that we only used rows 5 to 13.

Separate night sky spectra were not taken. This limits the usefulness of the spectra, especially in spectral ranges with a strong night-sky contribution like the near infrared. Also, no effort was made to correct for the underlying galactic absorption-line spectrum. We here only present those results from emission-line spectra which we believe to be essentially unaffected by any deteriorations.

3. Results

3.1. Broad-line component

The broad component of Hβ from the nuclear spectrum (S8) is shown in Fig. 1. It could be decomposed from narrow Hβ by a straightforward eye-fit made on the computer screen. The velocity widths of the broad component are FWHM = $1895\,\mathrm{km\,s^{-1}}$ and FWZI = $3586\,\mathrm{km\,s^{-1}}$. We obtained an intensity ratio broad/narrow of 2.05 which is close to the analogous ratio of 1.9 found in Paper I for Hα. Hence, we do not recognize any significant variation of the broad component relative to the four years earlier observing epoch reported in Paper I.

3.2. Circumnuclear narrow-line data

The most recent velocity field of NGC 1365 by the Swedish NGC 1365-group is given and interpreted in Lindblad et al. (1996b). Since we have not detected any noteworthy discrepancy we refrain from plotting the velocity curves deduced from our 5″ "long slits". Full widths at half maximum (FWHM) and line ratios of the narrow lines are given in Table 2. Near the nucleus, at the border of the high-excitation region, the ratio [OIII]λ5007/Hβ often varied drastically over the slit length. In these cases we give the range of the values (from west to east) measured along the 5″ effective slit length.

The line widths roughly agree with the values obtained in Paper I at much lower spectral resolution. This is due to the mostly inconspicuous quasi-Gaussian line shapes. For spectra S8, S6

Table 2. Results for narrow lines. In case of variations over the 5″long slit the range is given. FWHM in km s^{-1}. For S8, S6 and S7 FWHM range of [OIII]5007 and separately of Hβ in brackets. The line intensity ratios were measurable to $< 20\%$ accuracy.

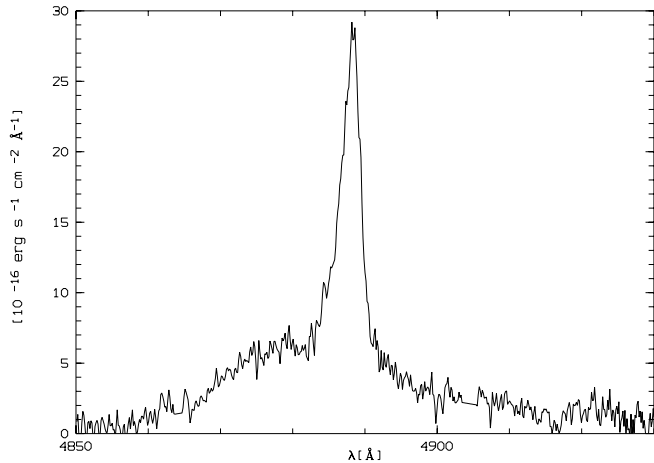| Frame	FWHM/(km s^{-1})	[OIII]5007/Hβ	[NII]6583/Hα	[SII]6716/Hα	[SII]6731/Hα
S8 (nucleus)	240–160 (140–160)	0.5–4.9	–	–	–
S1 (2″N 2″W)	180–170	–	0.61	0.12	0.12
S4 (2″S)	160–200	–	0.55	0.17	0.17
S5 (4″S)	170–50	–	0.58	0.28	0.25
S6 (5″S)	250–160 (130–210)	0.18–2.63	–	–	–
S7 (10″S)	250–180 (100–220)	0.14–1.41	–	–	–
S9 (20″W)	–	7.9	–	–	–
S2 (20″W)	–	–	2.3	0.39	0.33
S3 (20″W 2″S)	–	–	1.6	0.34	0.29

Fig. 1. Hβ from the nucleus, showing the peaked narrow component on top of an easily distinguishable broad component which is typical for a Seyfert 1.5 galaxy.

and S7 the slit crossed the boundary between the low-excitation star-formation region and the high-excitation [OIII] enhanced region which is presumably influenced by ionizing beams from the AGN continuum source. Here the line widths of [OIII]λ5007 and Hβ often differ drastically, signifying a mixture of at least two components with varying line ratios in velocity space. The difficulty of an unambiguous decomposition hampers a detailed interpretation of the [OIII]/Hβ line ratios. However, more complete spatial covering shows that line splitting occurs in some regions (e.g. Phillips et al. 1983; Edmunds et al. 1988). Most recently, Hjelm & Lindblad (1996) proposed a detailed decomposition of the velocity field which they modelled by a disk component plus biconical accelerated outflow. At the positions covered here, the 'red' ratios [NII]/Hα and [SII]/Hα turned out to be relatively constant over the slit lengths.

The circumnuclear line ratios essentially come from regions also studied in Paper I. Overall, we find good agreement and the same conclusion is valid that the line ratios lie on the borderline between active and HII-type objects in the diagnostic diagrams of Veilleux & Osterbrock (1987) as expected for a mixture of gas clouds with stellar and nonthermal ionization.

The spectrum across the nucleus (frame S8) provides a good example for the transition between the excitation classes in

[OIII]/Hβ. On the nucleus, we have [OIII]5007/H$\beta = 3$ and 180 km s^{-1} wide [OIII] lines while Hβ(narrow) is 220 km s^{-1} wide. At 2″ to the west of the nucleus, Hβ is only 140 km s^{-1} wide versus 240 km s^{-1} for [OIII]λ5007 and the line ratio is low (5007/H$\beta = 0.5$). To the east of the nucleus, the [OIII]5007/Hβ ratio increases, and Hβ, after first becoming still wider than [OIII], soon decreases and reaches the same width (160 km s^{-1}) after 3″ while the line ratio has reached a value of 5.

3.3. The enigmatic region II: shocks or photoionization?

The last three rows in Table 2 give line ratios for region II (as dubbed in Paper I), the region 20″W of the nucleus. The high [NII]λ6583/Hα ratio of 2.6 ± 0.3 found in Paper I is confirmed within the errors. The present work adds the large [OIII]/Hβ ratio of ~ 8. A comparison with comprehensive sets of models for emission-line clouds ionized by OB stars (e.g. Schulz & Fritsch 1994) shows that [OIII]/Hβ is too large for excitation by common OB-stars, in particular in combination with the large strength of the [NII] and [SII] lines. The simple reason for this is that strong low-ionization [NII] and [SII] lines require a low ionization parameter which automatically decreases the high-ionization [OIII] lines in case of 'thermal' input continua.

In fact, together with [OIII]/Hβ, [NII] and [SII] relative to Hα put region II into the AGN part of the diagnostic diagrams of Veilleux & Osterbrock (1987). An [OIII] enhancement in this region was earlier noticed by Edmunds et al. (1988; our region II overlaps with their regions 4 and 8) who had already suggested that here part of the wide NW counterpart of the SE ionization cone might be seen. Hjelm's & Lindblad's (1996) map of the cone does not extend that far away from the nucleus.

Altogether, this suggests that the gas is photoionized by the central AGN source. An alternative may be 'shocks with precursor' because such models produce AGN-like line ratios (Dopita & Sutherland 1995). We discuss both possibilities in turn.

3.3.1. Excitation via shocks?

Classical shock models (e.g. Shull & McKee 1979) would not produce line ratios like those observed in region II. However, Dopita & Sutherland (1995) computed synthetic spectra from

regions of *fast* shocks including a precursor HII region, which is *photoionized* by EUV photons generated in the hot post-shock plasma. In this way AGN-like line ratios can be produced. Putting the line ratios of region II into their diagnostic diagrams leads to a shock velocity of $\gtrsim 300 \, \mathrm{km \, s^{-1}}$ from [SII] and [OIII]. [NII] does not fall close to the model grid and the models would at least require a twofold nitrogen abundance increase to reproduce the 6583-line.

Although such models might be adjustable to fit the observed line ratios, the pertinent question arises how the necessary large speeds should arise in region II. Line widths far below $300 \, \mathrm{km \, s^{-1}}$, missing evidence for jet interaction (a radio jet has only been noticed towards the SE of the nucleus, in the direction of the SE outflow cone) provide a lack of support for such a picture. On the other hand, the closeness of the dust lane suggests the presence of bar shocks in the vicinity of region II although a comparison with the observed optical velocity field of the disk (Lindblad et al. 1996b) and hydrodynamical simulations (Lindblad et al. 1996a) shows that region II is not directly involved. In principle, photoionization by adjacent shock-induced EUV continua is conceivable but again the velocities in the bar models are not sufficient. Hence, missing positive evidence for shock-induced ionization we have to scrutinize the AGN scenario in turn.

3.3.2. Photoionization by isotropic nuclear radiation

Now the implications will be tested for the case that region II is ionized by the central AGN. The [SII]$\lambda 6716/\lambda 6731$ ratios given in Table 2 lead to an electron density $\log n_{\mathrm{e}} = 2.3 \pm 0.4$ for a single-density region (Osterbrock 1989). For fully ionized hydrogen dominated gas with hydrogen density n_{H} we have $n_{\mathrm{H}} \approx n_{\mathrm{e}}$. Following Ferland (1993), we define an ionization parameter U in the form

$$U = Q/(4 \, \pi \, r^2 \, c \, n_{\mathrm{H}}) \qquad (1)$$

(Q rate of hydrogen ionizing photons isotropically emitted by nuclear source, r distance between source and ionized gas). Our aim is to determine Q via Eq. 1 because this provides us with information on the AGN. At the adopted distance of NGC 1365, $20'' \,\hat{=}\, 1.9 \, \mathrm{kpc}$ in the plane of the sky or $r = 2.2 \, \mathrm{kpc}$ in the plane of NGC 1365 (for PA (l.o.n.) $= 220°$ and $i = 40°$ in accordance with Jörsäter & van Moorsel 1995) (slightly less for the new HST derived distance). For the determination of U we employed *Cloudy*, Ferland's (1993) versatile photoionization code. As input we used our standard mean AGN continuum (Komossa & Schulz 1997), $r = 10^{21.8} \, \mathrm{cm}$, input densities $n_{\mathrm{H}} = 10^2$ and $10^3 \, \mathrm{cm^{-3}}$, solar chemical abundances or the N abundance increased by a factor of 3. Ionization bounded clouds are assumed. We varied the flux of the input continuum so that $\log U$ covered the range -3.5 to -1.5. The model sequences are shown in Fig. 2 where the filled square represents the observed line ratios from S9 and S2.

Model series for the densities $n_{\mathrm{H}} = 10^2$ and $10^3 \, \mathrm{cm^{-3}}$ lie closely together, the lower density would only predict a slightly larger U. Fig. 2 shows that $\log U = -3$ yields an excellent fit,
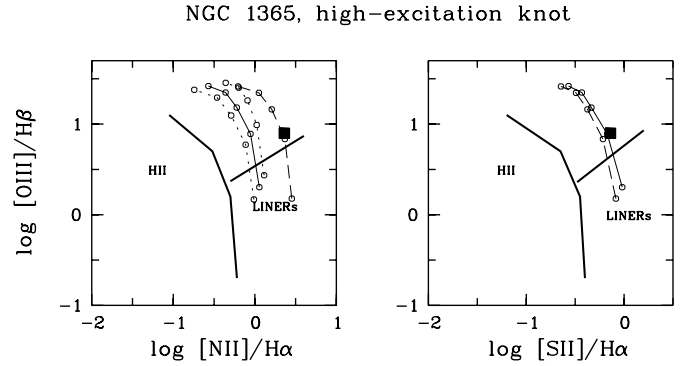
Fig. 2. Diagnostic emission-line intensity ratio diagrams from Veilleux & Osterbrock (1987) with [OIII]$\lambda 5007$/Hβ as ordinate; abscissa left: [NII]$\lambda 6583$/Hα, right: [SII]$\lambda\lambda 6716, 6731$/H$\alpha$. Borders separating the major excitation classes HII-region type objects, AGNs and LINERs are given. The filled square represents region II (20″ west of nucleus) in NGC 1365. Open circles connected by lines give model sequences along which the ionization parameter $\log U$ varies from -1.5 to -3.5 (in steps of 0.5 from top to bottom of each curve). For the dashed-line sequence the nitrogen abundance is 3 times enhanced relative to solar. Hydrogen densities (cgs units) were assumed to be $\log n_{\mathrm{H}} = 3$ for the solid and dashed line, and 2 and 4 for the left and right dotted curves, respectively.

provided that the nitrogen abundance is boosted by a factor 3. With Eq. 1, this fit leads to $Q = 1.3 \, 10^{54} \, \mathrm{s^{-1}}$, corresponding to $L(\mathrm{H}\alpha) = 9 \, 10^{41} \, \mathrm{erg \, s^{-1}}$ for $T = 2 \, 10^4 \, \mathrm{K}$. This is similar to the observed $L(\mathrm{H}\alpha) \sim 8 \, 10^{41} - 1 \, 10^{42} \, \mathrm{erg \, s^{-1}}$ of the classical nearby Seyfert NGC 4151 (Oke & Sargent 1968; Lacy et al. 1982). In Paper I we found a total luminosity of only $3.7 \, 10^{40} \, \mathrm{erg \, s^{-1}}$ from the central $2.''6 \times 6.''5$ in broad (65%) and narrow Hα. Applying a reddening correction with an extinction value at Hα of $A(\mathrm{H}\alpha) = 2.78$ taken from Alloin et al. (1981) we obtain a corrected $L(\mathrm{H}\alpha) = 4.7 \, 10^{41} \, \mathrm{erg \, s^{-1}}$, about half of the Q deduced $L(\mathrm{H}\alpha) \sim 10^{42} \, \mathrm{erg \, s^{-1}}$.

Given the crudeness of the estimates, a factor-of-two agreement is encouraging and a higher value of Hα extinction appears plausible so that consistency might be achieved. However, as recently pointed out by Komossa & Schulz (1998a,b), the true difficulty lies in the faintness of the X-rays in the 2–10 keV band which are even too faint compared to the *observed* Hα so that a complicated obscuration-scattering-anisotropy geometry has to be invoked if this AGN is intrinsically 'normal'.

4. Conclusions

The partially obscured active nucleus is surrounded by star formation regions. Steep gradients in line width and [OIII]/Hβ ratio across the nucleus suggest an apparently close symbiosis of nonthermal and thermal activity (Sect. 3.2).

A surprise is the detection of AGN-typical line ratios in faint emission-line gas from region II, a region 20″ west of the nucleus of NGC 1365. Although [OIII] enhancement in this region was earlier noticed by Edmunds et al. (1988) we have so far missed quantitative line ratios in the literature.

The conspicuous bar in this galaxy dominates the gas dynamics and suggests shock-induced excitation of region II. However, lacking positive evidence for velocities $> 300\,\mathrm{km\,s^{-1}}$ in the vicinity of this region we became reluctant about an interpretation in terms of shocks and explored the possibility that the high excitation gas belongs to the partially visible, wide bipolar SE-NW ionization cone. Considering the active nucleus of NGC 1365 as the only ionizing source of region II and assuming isotropic emission of the ionizing radiation, we estimated the intrinsic Hα luminosity of the AGN to be $\sim 10^{42}\,\mathrm{erg\,s^{-1}}$, of which only a few percent are observed in the innermost few seconds of arc. The minuteness of the observed line flux could be easily explained by a plausible range of Hα extinction of $3^{\mathrm{m}}5$ to 4^{m} which, however, would not provide a sufficiently thick gaseous absorbing column to explain the low 2–10 keV X-ray flux ($\tau = 1$ at 5 keV corresponds to $N_{\mathrm{H}} = 4\,10^{23}\,\mathrm{cm^{-2}}$ or $A_V = 220^{\mathrm{m}}$).

Hence, our picture of the central AGN in NGC 1365 is not without difficulties although current observational evidence appears to favor the AGN radiation-cone picture. To attribute a decisive role of shocks to the excitation of the gas in region II would be suggestive and cannot be completely ruled out, but lacks sufficient evidence at present. To safely distinguish between these two exciting scenarios, more detailed spatially resolved multiwavelength observations are required.

References

Alloin D., Kunth D., 1979, A&A 71, 335

Alloin D., Edmunds M.G., Lindblad P.O., Pagel B.E.J., 1981, A&A 101, 377

Blackman C.P., 1981, MNRAS 195, 451

Brindle C., Hough J.H., Bailey J.A., et al. 1990, MNRAS 244, 577

Burbidge E.M., Burbidge G.R., 1960, ApJ 132, 30

Burbidge E.M., Burbidge G.R., Prendergast K.H., 1962, ApJ 136, 119

Diaz A.I., Pagel B.E.J., Wilson I.R.G., 1985, MNRAS 212, 737

D'Odorico S., Ghigo M., Ponz D., 1987, ESO Scientific Report No. 6, ESO, Garching

Dopita M.A., Sutherland R.S. 1995, ApJ 455, 468

Edmunds M.G., Pagel B.E.J., 1982, MNRAS 198, 1089

Edmunds M.G., Taylor K., Turtle A.J., 1988, MNRAS 234, 155

Ferland G., 1993, Hazy, University of Kentucky, Internal Report

Hjelm M., Lindblad P.O., 1996, A&A 305, 727

Iyomoto N., Makishima K., Fukazawa Y., et al., 1997, PASJ 49, 425

Jörsäter S., Lindblad P.O., 1989, In: Meurs E.J.A., Fosbury R.A.E. (eds.) Extranuclear Activity in Galaxies. ESO Conf. Proc. 32, p. 39

Jörsäter S., Peterson C.J., Lindblad P.O., Boksenberg A., 1984a, A&AS 58, 507

Jörsäter S., Lindblad P.O., Boksenberg A., 1984b, A&A 140, 288

Jörsäter S., van Moorsel G., 1995, AJ 110, 2037

Komossa S., Schulz H., 1997, A&A 323, 31

Komossa S., Schulz H., 1998a, A&A 339, 345

Komossa S., Schulz H., 1998b, In: Aschenbach B., Freyberg M.J. (eds.) Highlights in X-ray Astronomy. MPE Report 269, in press

Kraan-Korteweg R.C., 1986, A&AS 66, 255

Kristen H., Jörsäter S., Lindblad P.O., Boksenberg A., 1997, A&A 328, 483

Lacy J.H., Soifer B.T., Neugebauer G., et al., 1982, ApJ 256, 75

Lindblad P.A.B., Lindblad P.O., Athanassoula E., 1996a, A&A 313, 65

Lindblad P.O., Hjelm M., Högbom J., et al., 1996b, A&AS 120, 403

Madore B.F., Freedman W.L., Silbermann N., et al., 1998, Nat 395, 47

Oke J.B., Sargent W.L.W., 1968, ApJ 151, 807

Osmer P.S., Smith M.G., Weedman D.W., 1974, ApJ 192, 279

Osterbrock D.E., 1989, Astrophysics of Gaseous Nebulae and Active Galactic Nuclei. University Science Books, Mill Valley, CA

Pagel B.E.J., Edmunds M.G., Blackwell D.E., Chun M.S., Smith G., 1979, MNRAS 189, 95

Pasquini L., 1993, CASPEC–Update to the Operating manual. ESO, Garching

Phillips M.M., Frogel J.A., 1980, ApJ 235, 761

Phillips M.M., Turtle A.J., Edmunds M.G., Pagel B.E.J., 1983, MNRAS 203, 759

Roy J.-R., Walsh J.R., 1988, MNRAS 234, 977

Saikia D.J., Pedlar A., Unger S.W., Axon D.J., 1994, MNRAS 270, 465

Sandqvist Aa., Jörsäter S., Lindblad P.O., 1995, A&A 295, 585

Schulz H., Knake A., Schmidt-Kaler Th., 1994, A&A 288, 425 (Paper I)

Schulz H., Fritsch Ch. 1994, A&A 291, 713

Shull J.M., McKee C.F., 1979, ApJ 227, 131

Stone R.P.S., Baldwin J.A., 1971, Cerro Tololo Contrib. No. 128

Storchi-Bergmann T., Bonatto C.J., 1991, MNRAS 250, 138

Teuben P.J., Sanders R.H., Atherton P.D., van Albada G.D., 1986, MNRAS 221, 1

Tüg H., 1977, ESO Messenger No. 11, p. 7

Veilleux S., Osterbrock D.E., 1987, ApJS 63, 295

Veron P., Lindblad P.O., Zuiderwijk E.J., Veron M.P., Adam G., 1980, A&A 87, 245

Ward M.J., Done C., Fabian A.C., Tennant A.F., Shafer R.A., 1988, ApJ 324, 767